ORIGINAL RESEARCH ARTICLE

Hydrogen as Carbon-Free Reducing Agent in Non-ferrous Slag Fuming

DESMOND ATTAH-KYEI, LASSI KLEMETTINEN, RADOSLAW MICHALLIK, JUSTIN SALMINEN, PEKKA TASKINEN, and DANIEL LINDBERG

In this work, pyrometallurgical treatment of non-ferrous iron residue was studied. This approach aimed to recover the valuable metals and convert the residue into reusable benign slag using hydrogen as a non-fossil reducing agent. The pyrometallurgical treatment for this type of residue involves pretreatment prior to two stages, oxidation and reduction. Hydrogen was employed as a reducing agent in slag cleaning. The reduction tests were performed at temperatures of 1200 °C, 1250 °C, and 1300 °C using H_2 and N_2 gases to form the reducing gas atmosphere. The results show that H_2 is an effective reductant because reduction proceeded rapidly, forming speiss droplets within the slag already after 10 minutes. The laboratory-scale experiments suggest that slags or other residues obtained from metallurgical processes can be further cleaned in a fuming process using hydrogen and its mixtures to obtain environmentally friendly cleaner slag with respect of volatile metals. The results also show that one can tune the reduction and control the formation of metallic iron during the process. Thermodynamic modeling was also performed to simulate the fuming stage, *i.e.*, reduction of the slag. Metal alloy formation as well as elemental distributions between metal and slag were studied, and results from thermodynamic modeling agree well with experimental results.

https://doi.org/10.1007/s11663-022-02640-0

I. INTRODUCTION

IN order to reduce the emission of CO_2 gas in the environment, the use of non-fossil reducing agents has become attractive in metallurgical processes. The use of hydrogen as a non-fossil reductant in metal production has been studied by several authors.[1–4] Hydrogen can be applied as a reducing agent for various oxides including nickel oxide, tungsten oxide, and iron oxide. Moreover, when H_2 gas is employed as a reduction agent, the reaction rate is faster compared to other reducing agents.[5,6] It has been reported that although producing hydrogen-based direct reduced iron is the most advanced technique and the most beneficial for the climate, this process is costly and involves large amounts of electrical energy when generating hydrogen by electrolysis. The steelmaker SSAB has formed a joint venture, HYBRIT, with LKAB and Vattenfall, where hydrogen is used as reducing agent in steel making. This technology is currently in the pilot phase and SSAB aims to bring fossil-free steel to the market by 2026.[7]

Bahgat and Khedr studied the reduction kinetics of magnetite single crystal using hydrogen at 900 °C to 1100 °C and concluded that reduction rate increases with temperature.[8] El Greassy *et al.* investigated hydrogen reduction of Fe_2O_3 samples with different porosity at temperatures from 700 °C to 1000 °C and reported increased reduction to high porosity and higher temperature.[9] H_2/CO/mixtures used in the iron oxide reduction showed that H_2 reduces iron oxide to lower forms faster and better than CO.[10–12]

During the production of zinc, large quantities of iron residue are released as side product.[13–15] Iron residue produced is usually landfilled at tailing dams.[16–18] Presently, about 85 pct of primary zinc is produced using hydrometallurgical route through roasting–leaching–electrowinning. During the process, jarosite [a mineral with the composition $KFe_3(SO_4)_2(OH)_6$, where K^+ can be exchanged for many other metals and ions, such as Na^+, NH_4^+, Pb^{2+}, Ag^+] is commonly used to regulate the level of iron in the solution by precipitation. Other harmful elements such as As, Cd, Zn, Pb, and Sb co-precipitate with jarosite or iron residue into the

DESMOND ATTAH-KYEI, LASSI KLEMETTINEN, PEKKA TASKINEN, and DANIEL LINDBERG are with the Department of Chemical and Metallurgical Engineering, School of Chemical Engineering, Aalto University, Kemistintie 1, P.O. Box 16100, 00076 Aalto, Finland. Contact e-mail: daniel.k.lindberg@aalto.fi RADOSLAW MICHALLIK is with the Geological Survey of Finland, Vuorimiehentie 2, 02150 Espoo, Finland. JUSTIN SALMINEN is with the Boliden Kokkola, Sinkkiaukio 1, 67101 Kokkola, Finland.

Manuscript submitted March 4, 2022; accepted August 24, 2022.
Article published online October 3, 2022.

jarosite matrix, and therefore the material is classified as hazardous. The residue is also not usually pure jarosite but mixed with various sulfur precipitates from direct zinc sulfide leaching.[19,20] The iron residue contains significant concentrations of compounds of iron, zinc, lead, cadmium copper, antimony, and minor concentrations of precious metals such as gold and silver, which can be recovered.[20–22] Due to the presence of these valuable metals as well as stricter environmental regulations and higher cost associated with land filling, using this residue as a secondary raw material is a promising alternative. It is important to regain valuable elements and also remove the harmful elements from the residue before discarding or using it for example as aggregate road construction.[21,23–25] This residue is mainly generated in Finland, Norway, Germany, Belgium, Holland Argentina, France, Canada, Spain, Australia, Korea, Mexico, and Japan.[26]

In order to gain both value and reduce the environmental impact of this residue, thermal treatment is preferred. Pyrometallurgical treatment of iron residue is applied at Korea Zinc Facility in Onsan, South Korea, where the residue together with reductant coal and flux are smelted to produce fume and slag. The valuable metals such as Zn, Pb, Ag, Cd, and In are recovered from the fume and depending on the input and operating conditions, in the metallic phase.[24,27,28]

Another example of a pyrometallurgical processing route of the leach residue consists of three stages; pretreatment, oxidation, and reduction.[29] In the pretreatment stage, the dried sample is thermally decomposed into simpler compounds. OH groups and SO_4 groups are removed together with the evaporation water present in the jarosite. Oxidation is performed to convert the metals to their highest oxidation states, as well as to decrease the sulfur concentration to less than 1 wt pct. After oxidation, a reduction step is carried out, where the hazardous metals are removed by volatilization. Different phases including gas, slag, and liquid metal (speiss) are formed. Process parameters can be adjusted to obtain the optimum distribution of elements, *i.e.*, to deport the valuables to the speiss as efficiently as possible.

In this work, the use of hydrogen as a reducing agent in pyrometallurgical reduction of the oxidized slag from zinc smelting iron residue was studied. Several studies have been done using different reductants. Toropainen[30] used MTDATA to simulate the conversion of iron residue into slag and recovery of valuable metals through pyrometallurgical techniques using carbon as reducing agent. They reported that at 1 atm pressure and 1300 °C, Cd, Pb, and Zn partly evaporate, while As, Cu, and Sb deport to speiss which is a mixture of liquid iron and As–Fe. In the study of Nurmi,[31] CO–CO_2 was used as reductant in a two-stage oxidation–reduction treatment of residue from zinc processing and showed the formation of speiss containing Cu, Sb, Pb, Fe, As after 120-min reduction. Rinne[27] determined the feasibility of using spruce biochar as reductant as compared to coke in thermal treatment of iron residue and reported the formation of speiss after 20-min reduction. The author stated that compared to coke, biochar improved the volatilization rate of Pb, As, and Sb and attributed the better performance to high reactivity of biochar which improves reduction kinetics.

This study investigates the effects of temperature and reduction time on the recovery of valuable metals and production of benign slag to be safely discarded or used in road construction.

II. EXPERIMENTAL

The dried iron residue samples were pretreated at 700 °C for 1 hour using 65 mL/min air flow in 10-g batches. The residue thermally decomposes at the stage and its sulfur content decreases as well. Several batches were pretreated and mixed to ensure homogeneity. Chemical analysis was performed for the thermally pretreated sample, and silica sand (Sigma Aldrich, 274739) was added to adjust the Fe/SiO_2 ratio to 1.86 (w/w). This was done to lower the melting point of the residue and to enhance the distribution of valuable elements to the alloy/speiss phase during reduction stage.[32] 2 g of the pretreated leach residue, mixed with silica sand, was placed in an MgO crucible (inner diameter 1.5 cm, height 2.5 cm) (Tateho Ozark, Webb City) and lifted into the furnace using a platinum wire which was hanged from the top of the furnace. The furnace was already heated to the specified temperature. Gas flow rates were controlled by rotameters (R in Figure 1) (Kytölä Instruments, Jyväskylä, Finland), and temperature was measured by a calibrated S-type thermocouple (Johnson-Matthey, UK) connected to a Keithley multimeter.

Oxidation was carried out using 65 mL/min oxygen (99.999 vol pct) flow for 60 minutes.[27] After oxidation, the reduction step was performed for 5, 10, 15, or 20 minutes. Oxidation is important to remove sulfur present in the slag to mitigate the tendency of producing FeS or iron matte which traps valuable metals like Ag making it difficult to retrieve the valuable metal. Moreover, Hoang reported that based on thermodynamic calculations, 99 pct of Zn in pure ZnS material is converted to metal vapor during oxidation.[20] Prior to reduction, the furnace was purged with nitrogen (99.999 vol pct) for approximately 30 minutes to remove all the oxygen and any released gas components from the system. The gas mixture used during reduction was a mixture of hydrogen and nitrogen with 20 vol pct hydrogen (99.995 vol pct) and a total flow rate of 400 mL/min. Higher H_2 pct resulted in rapid formation of iron sheet on top of the sample, preventing any further reduction of the sample. Oxidation and reduction tests were done at 1200 °C, 1250 °C, and 1300 °C. These temperatures were selected in order to compare the results to previous works on iron residue reduction.[27,29–31] Another set of tests were done at 1300 °C where the samples were left in the furnace under inert conditions (320 mL/min nitrogen flow) for one hour after carrying out reductions for the different times.

After reduction, each sample was quenched in ice water. All the gases used in the tests were purchased from Aga-Linde Oy (Finland).

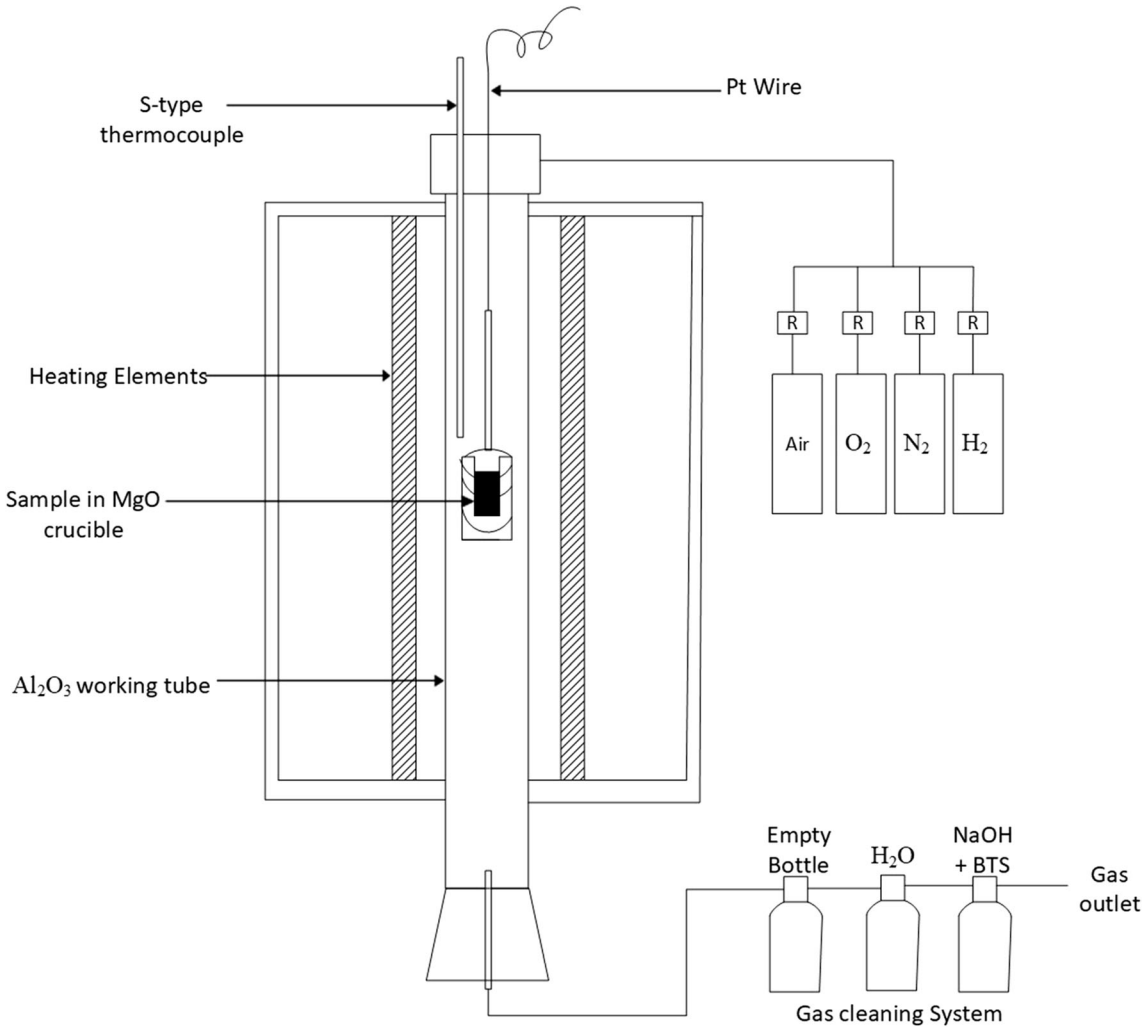

Fig. 1—Schematic of experimental setup used for the study.

After quenching, the samples were cast in epoxy, polished, and carbon coated for electron probe microanalysis (EPMA; Cameca SX-100, France). The accelerating voltage and beam current were 20 kV and 60 nA, respectively. A defocused 20 μm beam was used for the slag phase and some of the speiss areas. For smaller speiss droplets as well as the spinel, a focused beam was used. Standardization of the characteristic X-ray lines to be measured for the individual elements were carried out by using natural and synthetic minerals obsidian for Si Kα and O Kα, tugtupite for Na Kα, almandine for Al Kα, diopside for Mg Kα and Ca Kα, sanidine for K Kα, pentlandite for S Kα, hematite for Fe Kα, rhodonite for Mn Kα, arsenopyrite for As Kβ, sphalerite for Zn Kα, barite for Ba Lα, galena for Pb Mα and antimony telluride for Sb Lα, as well as pure metals cobalt for Co Kα, nickel for Ni Kα, copper for Cu Kβ, silver for Ag Lα. Totals of the individual phase analyses after PAP-ZAF matrix correction were generally 99 $\pm$ 2 wt pct.

The bulk chemical compositions before and after pretreatment were analyzed with inductively coupled plasma-optical emission spectroscopy (ICP-OES), with iCAP 6000 series, Thermo Fisher Scientific type apparatus. The samples were prepared for the analysis with microwave digestion (MARS6 microwave digestion system, CEM Corporation) using a mixture of HNO_3, HCl, and HBF_4 as the digestion medium.

III. RESULTS AND DISCUSSION

A. *Pretreatment of Iron Residue*

The iron residue breaks down during the pretreatment stage. Several authors have studied the thermal decomposition of the iron residue and reported a three-step mechanism; evaporation of water, dehydroxylation, and desulfurization.[27,33,34] Table I shows the composition of the iron residue starting material that was pretreated thermally and after oxidative smelting.

Table I. Mass Percentage of Chemical Composition of Iron Residue After Pretreatment and After Oxidation at 1200 °C Obtained from ICP-OES, Wt Pct

Element	Al	As	Bi	Ca	Fe	K	Mg	Mn
Pretreated Iron Residue	1.4	1.4	0.023	8.0	28.8	0.33	0.07	0.04
After Oxidative Smelting	0.77	1.3	0.024	7.2	32.5	0.25	2.3	0.04
Element	Na	Pb	S	Sb	Se	Si	Zn	
Pretreated Iron Residue	2.5	4.7	14.0	0.11	0.0028	3.4	1.4	
After Oxidative Smelting	1.8	4.9	0.46	0.12	< 0.001	9.8	1.4	

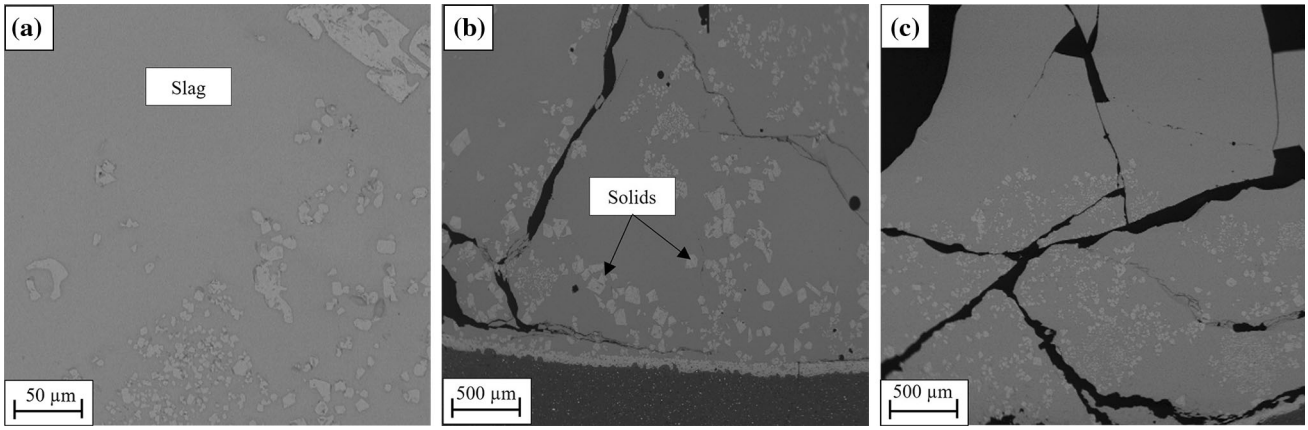

Fig. 2—Micrographs of the iron residue after oxidation step at (*a*) 1200 °C, (*b*) 1250 °C, and (*c*) 1300 °C for 1 hour containing molten slag and iron oxide.

B. *Oxidation Tests*

Previous studies on pyrometallurgical treatment of the iron residue suggested an oxidation step prior to reduction.[27,31,35] Oxidation of residue was performed to melt the sample and convert the metals present in the residue to oxides in a slag as well as decrease sulfur content to less than 1 wt pct.

SEM analysis revealed that after oxidation, solid iron oxide is dispersed within the molten slag at the different temperatures. The light gray regions shown in Figure 2 are composed of iron oxide (Fe_3O_4) and are scattered within the otherwise homogeneous molten slag (darker gray areas).

The molten slag consists largely of oxides of Fe, Si, Ca, and Pb. The dark regions are cracks found within the samples and attributed to the thermal shock experienced during quenching.

The analysis revealed that the sulfur concentration significantly decreases in the slag at all temperatures of this stage, which suggests sufficient contact between the oxygen and the sample. While Steinlechner and Antrekowitsch[34] ascribed the notable decrease in sulfur content to decomposition of iron residue to release SO_3, oxygen reacts with elemental sulfur or metal sulfide which may be present in the feed material at the high temperature. As temperature increased, reactions between slag and MgO crucible became more rapid, increasing the MgO contents in the solids and in the slag.

C. *Reduction Tests*

The objective for reduction step was to reduce the metal oxides formed during oxidation stage, using hydrogen. Volatile metals such as lead are expected to vaporize in the gas stream during reduction, thus decreasing the percentage of Pb in the slag.

The various elements present in the residue distribute into different phases including gas, slag, spinel (solid), and metal. The heavier metallic droplet, called here speiss due to its composition, was formed and settled at the bottom of the crucible. The speiss consists of metal (typically Fe or Ni) arsenides or antimonides. While the formation of speiss in non-ferrous smelters is unwanted because it dissolves large quantities of precious metals and copper, in the treatment of zinc leach residue it proves to be advantageous, since it collects valuable metals from the slag.[36–38] Moreover, harmful elements that are undesirable in the slag and do not vaporize completely, such as Pb, deport in the metal alloy phase instead of the slag.

SEM micrographs of the reduction test at the different temperatures (Figures 3, 4, and 5) showed that, after 5 minutes of H_2 blowing, no metal droplets were found from the sample. However, small speiss droplets were found for reductions of 10 minutes and longer. The formed metal droplets were heterogenous after quenching and had areas that were rich in lead with other areas rich in As and Cu. In a previous study, the speiss formed during reduction of slag consisted mainly of copper, antimony,

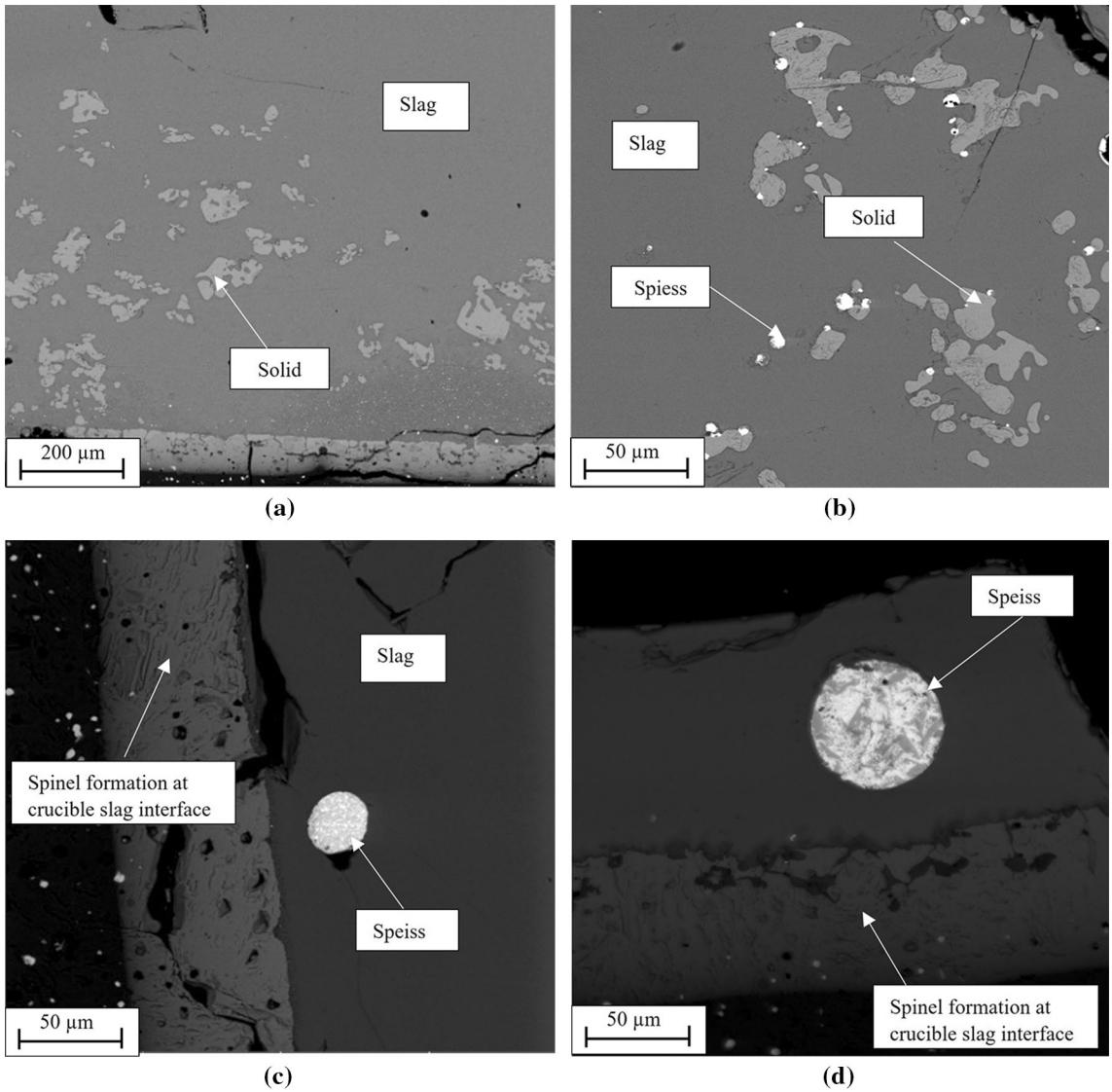

Fig. 3—Micrographs of quenched iron residue post reduction at 1200 °C after (*a*) 5, (*b*) 10, (*c*) 15, and (*d*) 20 minutes.

and lead.[31] EPMA analysis of the sample reduced at 1200 °C revealed that after 10 minutes, the speiss consists of 88 pct Pb with 4.25 and 2.66 pct Sb and As, respectively. 15- and 20-min reduction, however, had lower Pb pct and > 40 and > 7 pct As and Sb, respectively.

The formation of metal droplets after 10 minutes for all the temperatures suggests that hydrogen is an effective reductant. In Nurmi's work where the reduction of iron residue was studied using 260 mL/min CO/CO_2, the speiss phase was formed after 120-min reduction. Rinne found that speiss is formed after 20 minutes when blend of coke and biochar in a ratio 50 to 50 pct is used as reductant in pyrometallurgical treatment. The use of hydrogen has faster reaction kinetics leading to speiss formation that forms iron residue in a shorter time compared to coke, biochar, and CO/CO_2.

It was expected that most of the lead would vaporize at the experimental temperatures. However, the speiss formed had Pb-rich areas, the amount of which generally decreased at higher temperatures. This indicates a higher degree of Pb volatilization when the temperature increases. Pb is likely trapped (embedded) within the slag and does not easily break out into the off gas.

The solids formed during oxidation, consisting of predominantly iron oxide (Fe_3O_4), is assumed to be reduced by hydrogen to FeO at the reduction stage and dissolved in the molten slag. Iron oxide was seen at the rim of the crucible (slag and crucible interface) after 15 minutes. The MgO crucible dissolves at high temperatures into the slag as reduction takes place and probably forms some kind of ferrous based spinel [$(Fe, Mg)(Fe)_2O_4$] at the interface of the slag and crucible.

At 1250 °C, the SEM–EDS micrographs show less solid iron oxide in the slag than initially. Homogenous slag, free of solids (iron oxide) was produced after 10 minutes and longer reduction. EPMA analysis of reduction sample at 1250 °C and 1300 °C reveals that Pb percentage in speiss is lowest at 15-min reduction. Apart from 10-min reduction at 1250, Sb percentage within metal was around 5 pct.

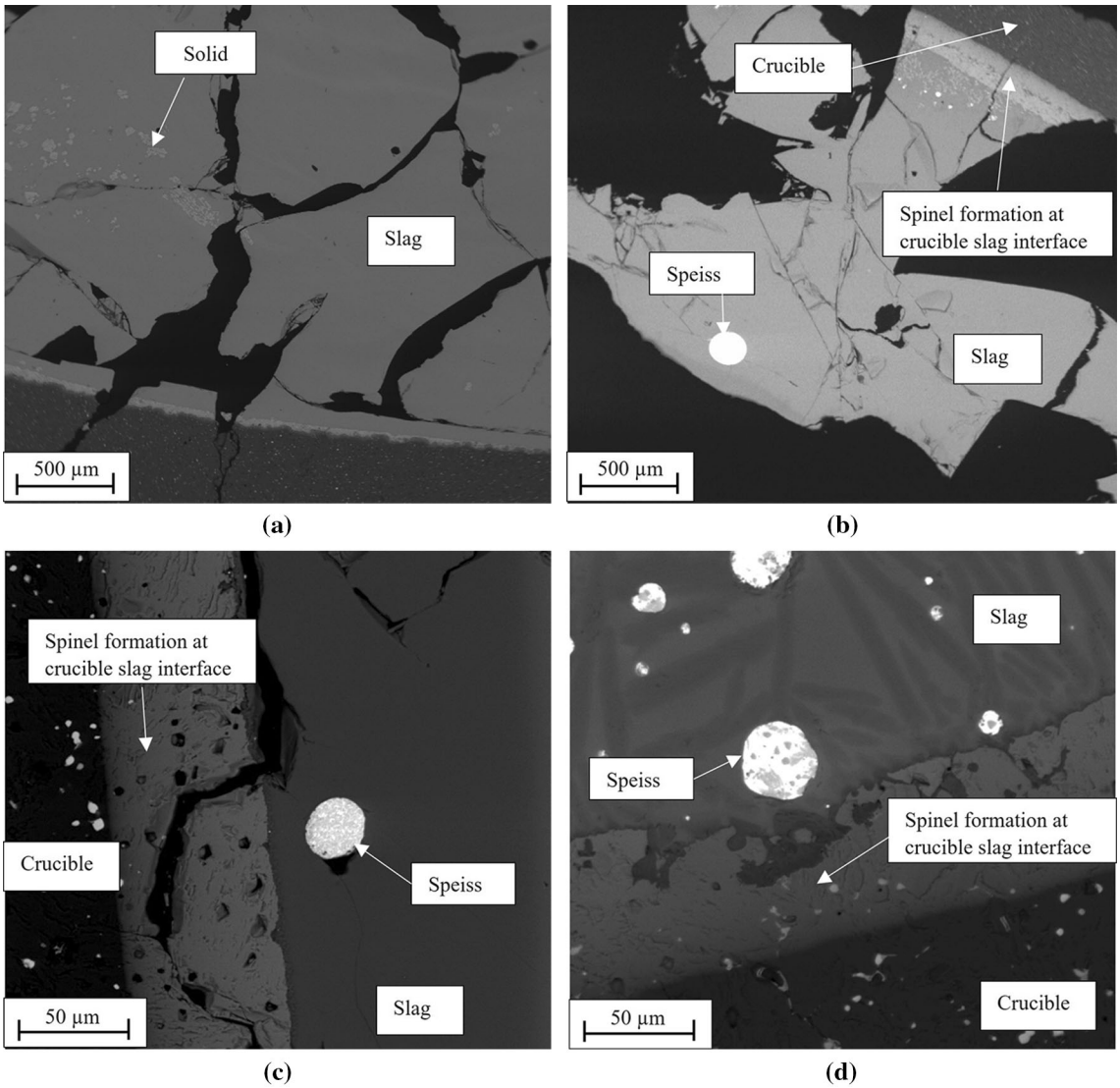

Fig. 4—Micrographs of iron residue after reduction at 1250 °C after (*a*) 5, (*b*) 10, (*c*) 15, and (*d*) 20 minutes.

In addition to the standard reduction tests at 1300 °C, another set of reductions was performed at 1300 °C, as shown in Figure 6. In this set, the samples were left in the furnace under inert conditions for 1 hour after carrying out reductions for the different times. This was done to quantify whether the volatilization of certain elements increased, as well as to see if the separate speiss droplets would coalesce into bigger droplets and to ascertain whether the sample behaves as predicted by subsequent thermodynamic model. It was observed that the concentrations of volatile elements in the slag phase were lower than in the tests without one-hour annealing under inert conditions, as expected. However, no significant differences were observed regarding the coalescence of smaller speiss droplets. After 15-min reduction and one hour under inert conditions, the micrograph reveals the presence of speiss with Fe–As regions combined with a Pb-rich area. This observation is in agreement with the thermodynamic calculations presented in the next section. Thermodynamic modeling performed using FactSage predicts the formation of two liquid metal phases (a miscibility gap) at oxygen partial pressures below than $10^{-9.6}$ atm.

The concentrations of Pb, As, and Zn in the slag phase as functions of reduction temperature and time are presented in Figure 7. The concentrations of all these elements decrease when the reduction time increases and when the temperature increases. The beneficial effect of inert atmosphere dwelling for 1 hour after reduction are clearly visible for Pb, As, and Zn. It was expected that the concentrations of Pb, As, and Zn decrease as time and temperature increase as they volatilize into the gas phase or deport to the speiss. However, there are some inconsistencies in the Pb and Zn concentrations in the slag. This may be attributed to the error that may have taken place during sampling the feed material used as the input.

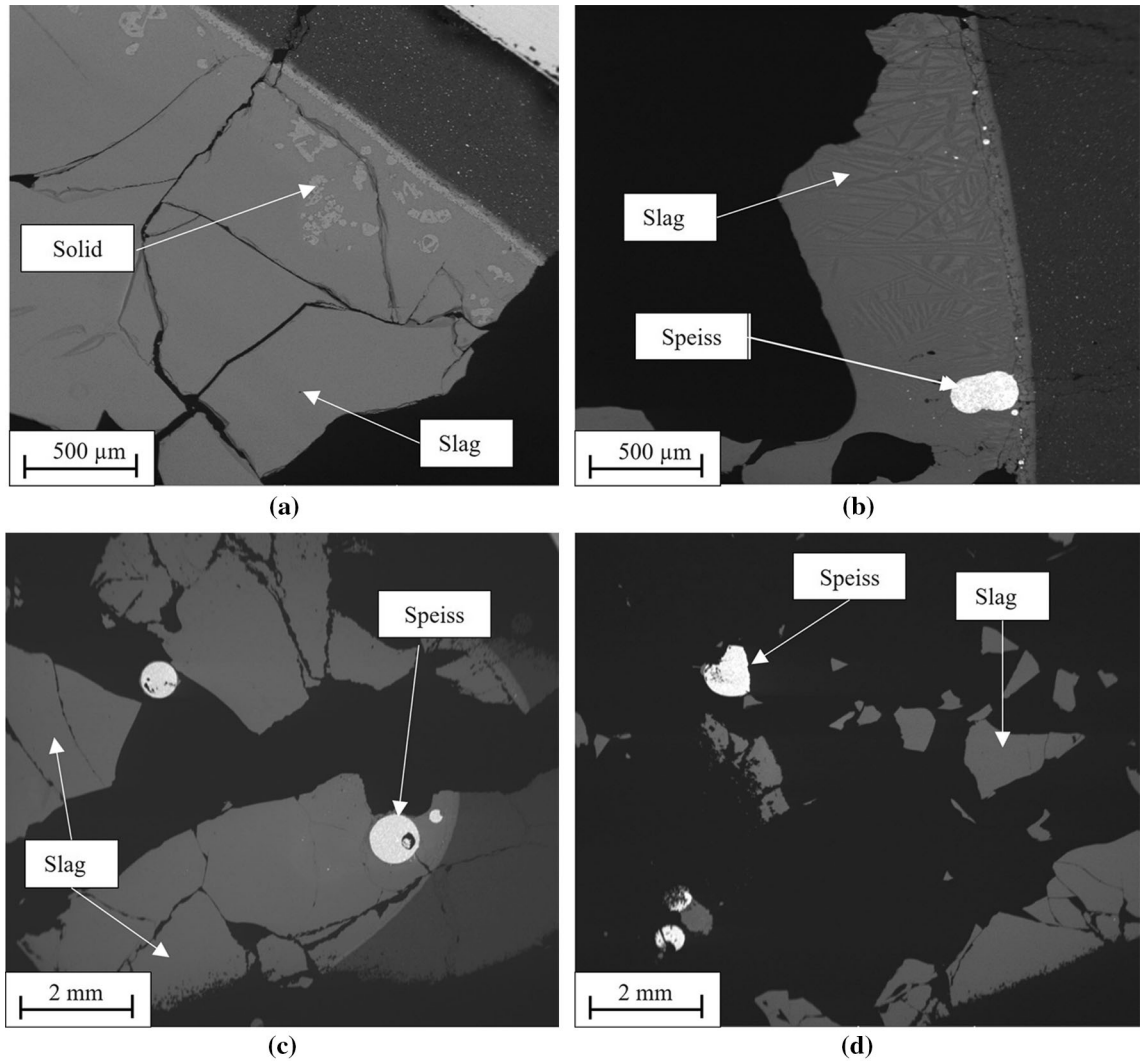

Fig. 5—Micrographs of iron residue after reduction at 1300 °C after (*a*) 5, (*b*) 10, (*c*) 15, and (*d*) 20 minutes.

The formation and distribution of the different species during reduction are shown in Figure 8. It is observed that after oxidation, solid (iron oxide) is formed and scattered within the slag. As reduction progresses, metal droplets (speiss) which are rich in Pb are produced. Iron oxide reduces to lower forms of oxides. The results from SEM analysis show speiss or metal droplet consisting of Fe–As-rich area attached to Pb-rich area. Pb subsequently vaporizes and the metal droplet is mainly FeAs speiss. The gray area represents the slag phase.

D. *Thermodynamic Modeling*

Reduction of iron residue was studied using the FactSage thermodynamic software package, version 8.0.[39] Elemental analysis performed on the products obtained from the oxidation step (Table I) was used as input in the software. The databases used for the calculations were custom collected based on the databases FactPS (Pure substances), FToxid (optimized for oxide systems), FSCopp (optimized for copper-containing solid and liquid alloys), as well as some data from the SGTE pure substance databases. The phases selected for the calculations were the spinel (solid solution phase with stoichiometry AB_2O_4, A, B = divalent and trivalent metals), slag (liquid oxide silicate phase), monoxide phase (solid solution), FCC, BCC, HCP-A3 (three solid multicomponent alloys), zincite (ZnO-based solid solution), PbO–ZnO solid solution, feldspar solid solution, and liquid metal. Ideal gas and pure solids were also selected before the calculations were done.

1. *Composition of reduction products at different oxygen partial pressures*

The phase equilibrium was predicted as a function of oxygen partial pressure. Figure 9 shows the results of $P(O_2)$ between 10^{-5} and 10^{-12} within which either solid Fe oxides (spinel) or solid metal (Fe) are stable. The conditions of interests are partial pressures of oxygen where only slag or slag + liquid metal is stable. In addition, the formation of gas phase is minimal and does not fully reflect the volatilization behavior of the various elements.

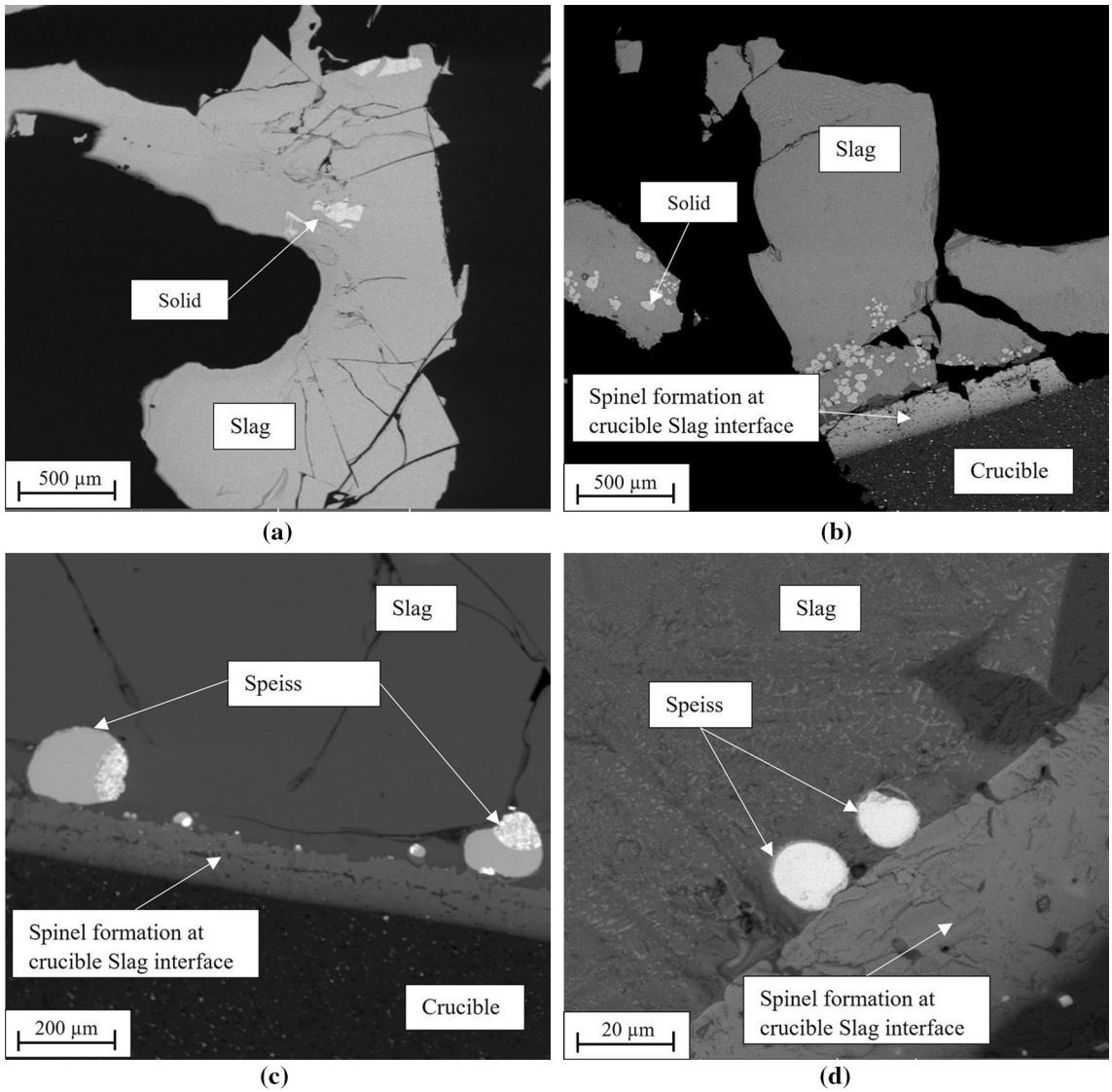

Fig. 6—Micrographs of post reduction at 1300 °C after (*a*) 5, (*b*) 10, (*c*) 15, and (*d*) 20 minutes and 1 hour of annealing under inert conditions.

The results (Figure 9) show that at higher oxygen partial pressure ($> 10^{-6.8}$ atm), the main products are slag and spinel. As reduction degree increases (decreasing oxygen partial pressures), FactSage predicts the presence of slag only between 10^{-7} and 10^{-8} atm. Liquid metal starts to form at oxygen partial pressure lower than 10^{-8} atm. Another liquid metal phase forms around $10^{-9.6}$ atm. When reduction continues to less than $P(O_2) = 10^{-11.2}$ atm solid metal, predominantly (> 98 pct) Fe was predicted to precipitate from the slag. The generation of solid iron is undesirable in the process, as valuable elements, such as Cu will dissolve in it and are very difficult to separate efficiently. With reference to Figure 9, it is important that the $P(O_2)$ be in the range $10^{-11} > 10^{-8}$ in order to produce speiss while avoiding the formation of solid iron.

Figure 10 shows the mass fractions of the main elements in the liquid metal phases formed. The main components of liquid 1 are Fe and As. Between $P(O_2)$ of $10^{-9.5}$ and the 10^{-11} atm, Fe increases from 30 to 85 pct, arsenic decreases to 10 pct and maintains the composition at $< 10^{-11}$ atm oxygen partial pressure. Pb formed disappears before $P(O_2)$ of 10^{-11} atm. Liquid 2 is mainly composed of Pb and As.

The mass fractions of four elements Pb, As, Zn, and Cu in the molten slag at 1300 °C are shown in Figure 11. The results show that the mass of Pb in the slag decreases the most from 8.5 to < 1 pct as the oxygen partial pressure decreases. Zn percentage in slag remained fairly around 1.4 pct and increased slightly after 10^{-11} oxygen partial pressure although the total mass of Zn in slag decreased around that point.

The distributions of four elements of interest (Pb, As, Zn, Cu) in the different phases are shown Figure 12. Pb in the slag is converted to liquid metal at $P(O_2) < 10$ 8 atm. As is only present in the slag phase between 10^{-8} and 10^{-6} atm $P(O_2)$. Lower than 10^{-8} As is gradually converted to liquid 1 (metal) and subsequently to liquid 2. At $> 10^{-6}$ atm oxygen partial pressure, FactSage

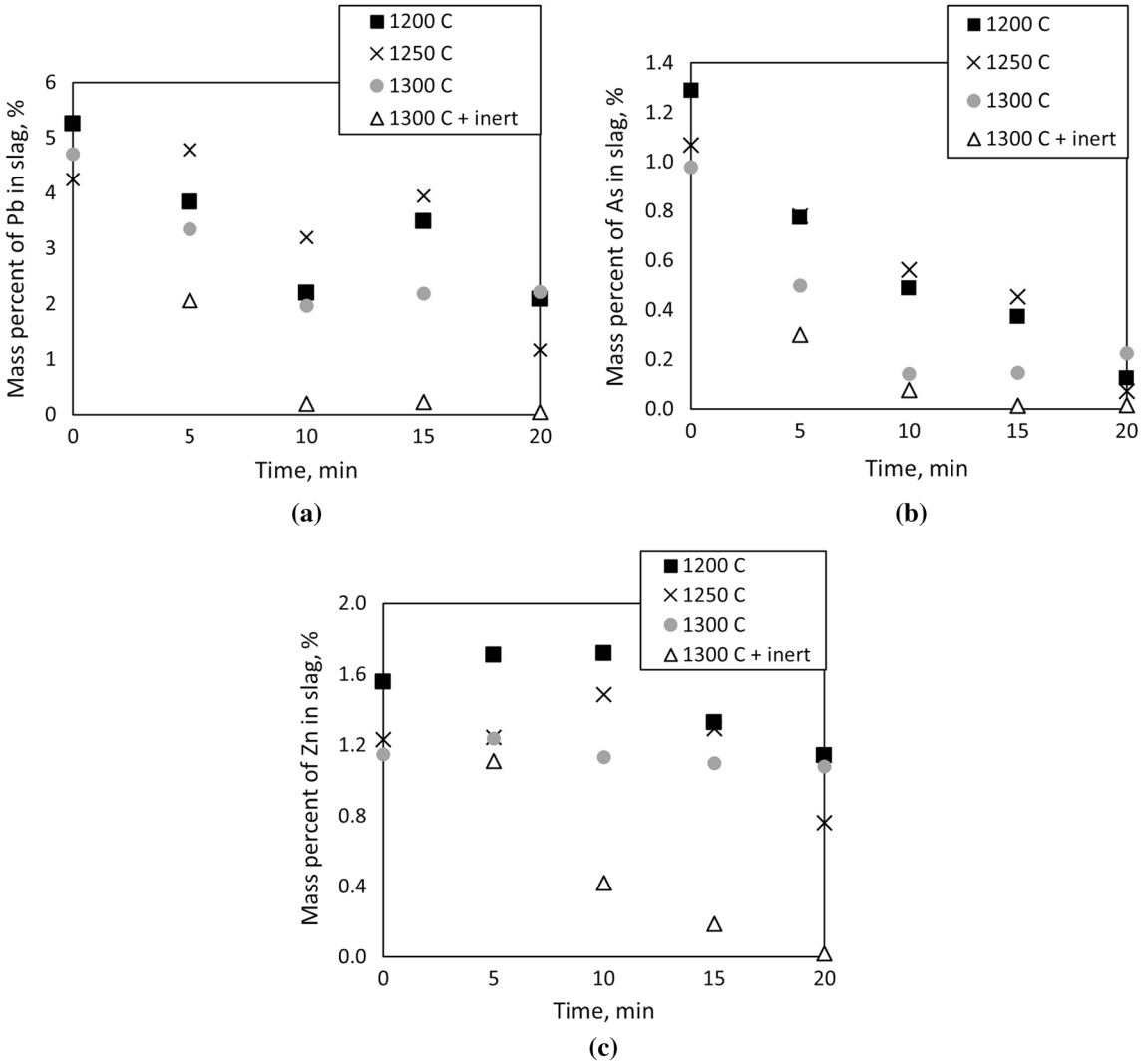

Fig. 7—Mass percentages of (*a*) Pb, (*b*) As, and (*c*) Zn, in the molten slag phase after reduction tests obtained by EPMA.

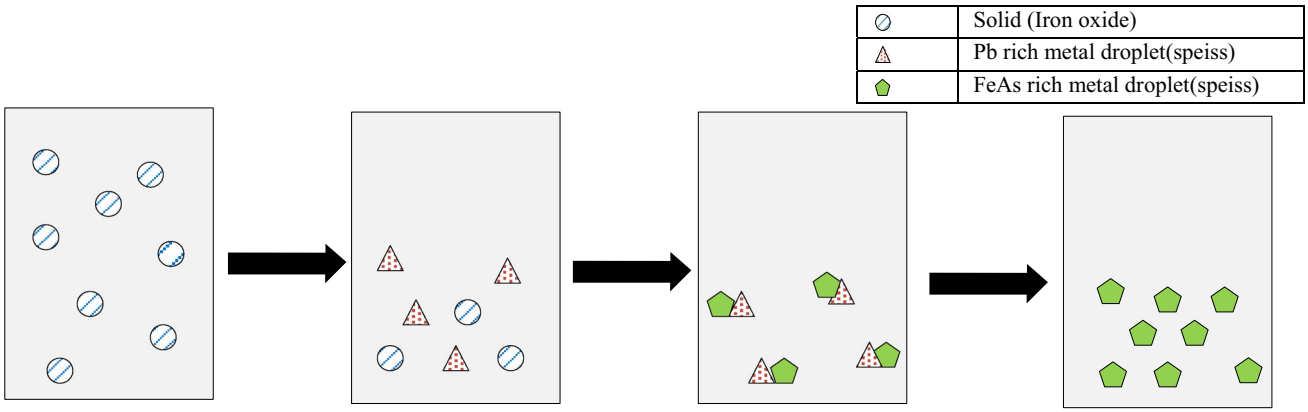

Fig. 8—A representation of the formation and distribution of species (speiss) within the slag during reduction.

predicts that As is present in the molten slag phase. Although Zn was expected to vaporize into the gas phase, it is mainly present in the liquid slag and partly found in the liquid alloy phase in $< 10^{-11}$ $P(O_2)$. This might be attributed to the low pressure, moreover, there was no blowing of gas.

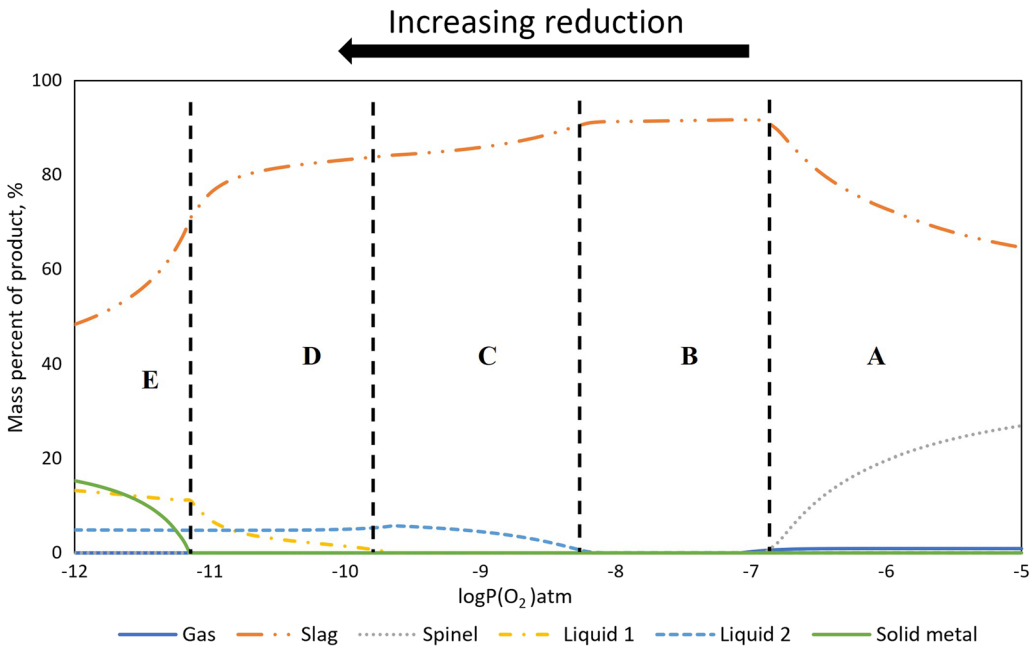

Fig. 9—Mass of phases obtained from reduction at 1300 °C for $P(O_2)$ between 10^{-5} and 10^{-12} atm.

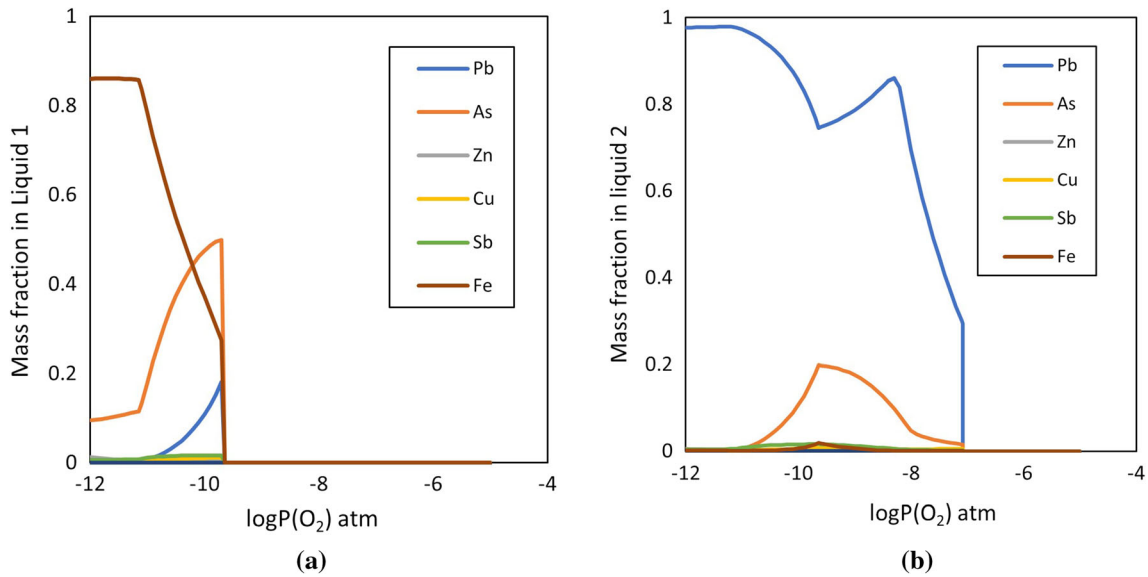

Fig. 10—Composition of (*a*) liquid 1 and (*b*) liquid 2 obtained from reduction at 1300 °C for $P(O_2)$ between 10^{-5} and 10^{-12} atm.

2. *Thermodynamic modeling using experimental conditions*

The conditions used during the reduction at 1300 °C were used as input in FactSage in order to predict the expected products. The open calculation option in FactSage was used for simulating the reduction of impure slag (after oxidation). In the open calculation mode, several stepwise calculations are performed. An incremental amount of an unreacted gas phase (*e.g.*, mixture of Ar and H_2) is added to the system (*e.g.*, fixed amount of slag) at fixed P and T, and the equilibrium compositions for the new system (*e.g.*, gas + slag) are calculated. Subsequently, the formed gas phase is removed from the system, and a new incremental amount of unreacted gas is added to the equilibrated solid and liquid phases from the previous step. This procedure can be repeated as many times as needed. By recalculating the gas amount to a gas flow, and normalize it to the initial solids amount, it is possible to relate the calculations to an ideal case of a time-dependent experiment, assuming all added gas is allowed to react with the condensed phases. 100 g of impure slag was reacted with a mixture of H_2 and an inert gas. The products formed, with the exception of the gas

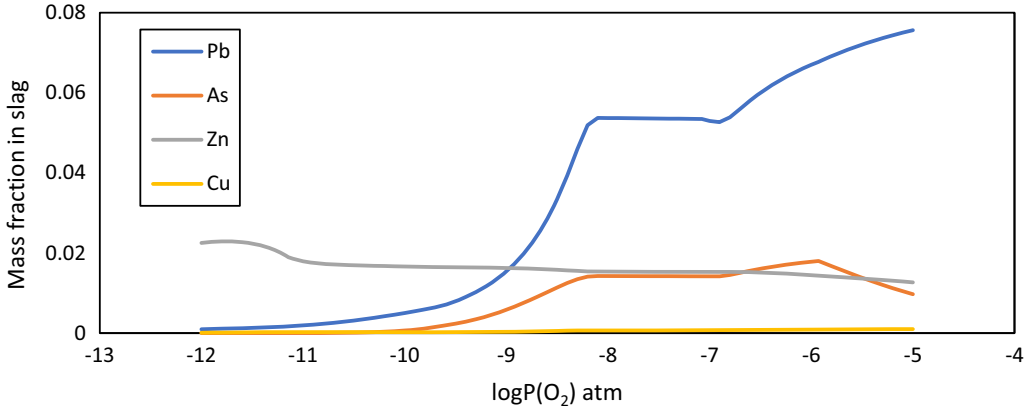

Fig. 11—Mass fraction of elements of interest in slag obtained from reduction at 1300 °C for $P(O_2)$ between 10^{-5} and 10^{-12} atm.

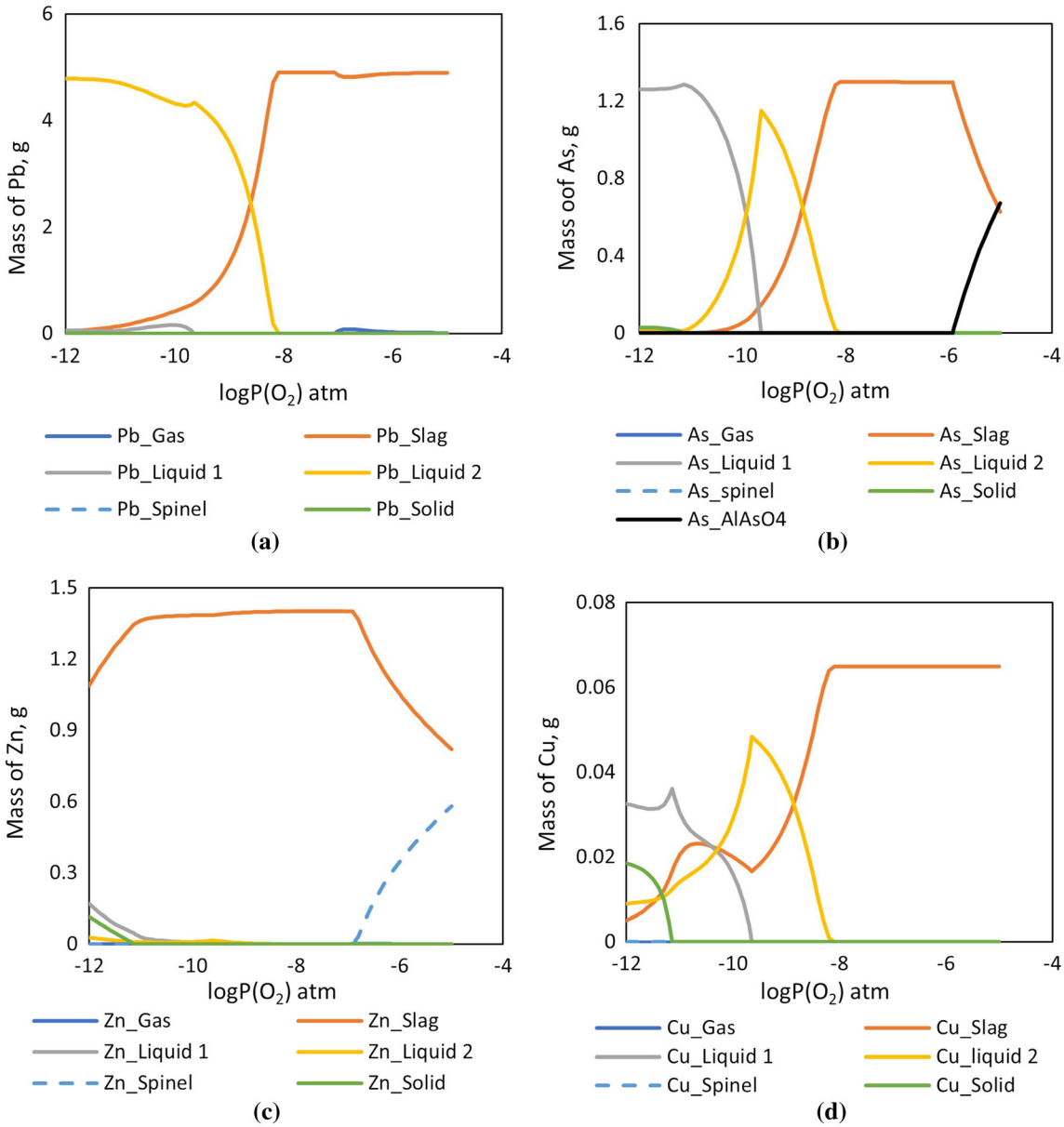

Fig. 12—Elemental distribution of (*a*) Pb, (*b*) As, (*c*) Zn, and (*d*) Cu obtained from reduction at 1300 °C for $P(O_2)$ between 10^{-5} and 10^{-12} atm.

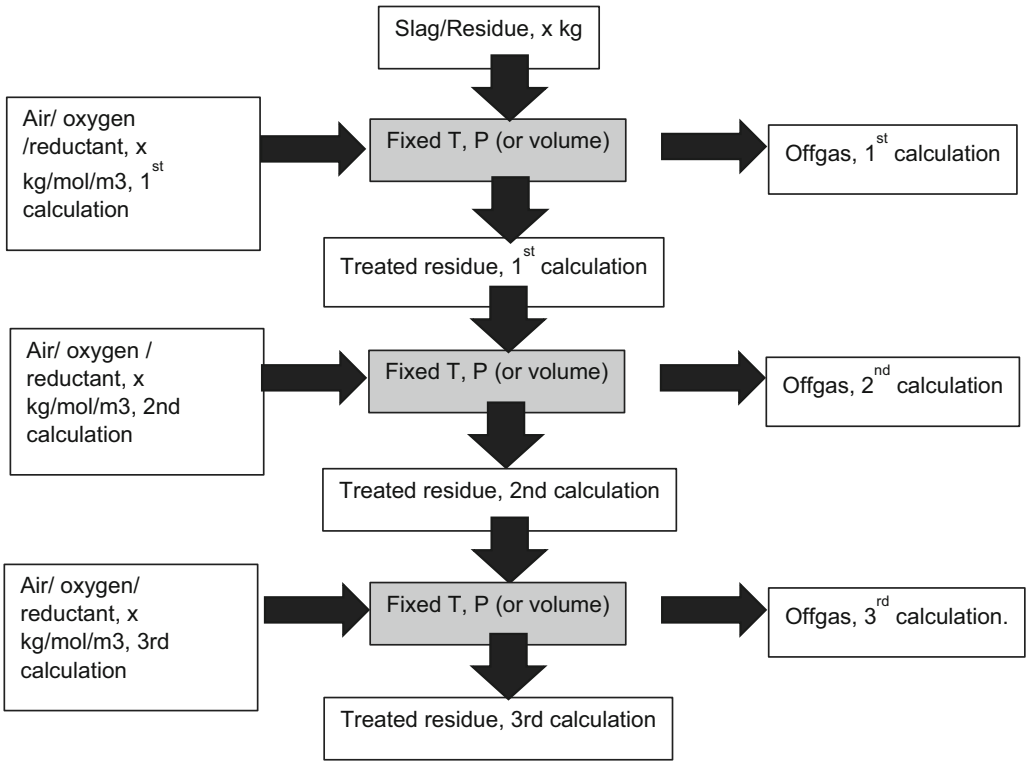

Fig. 13—Flow diagram showing how open calculations were performed using FactSage.

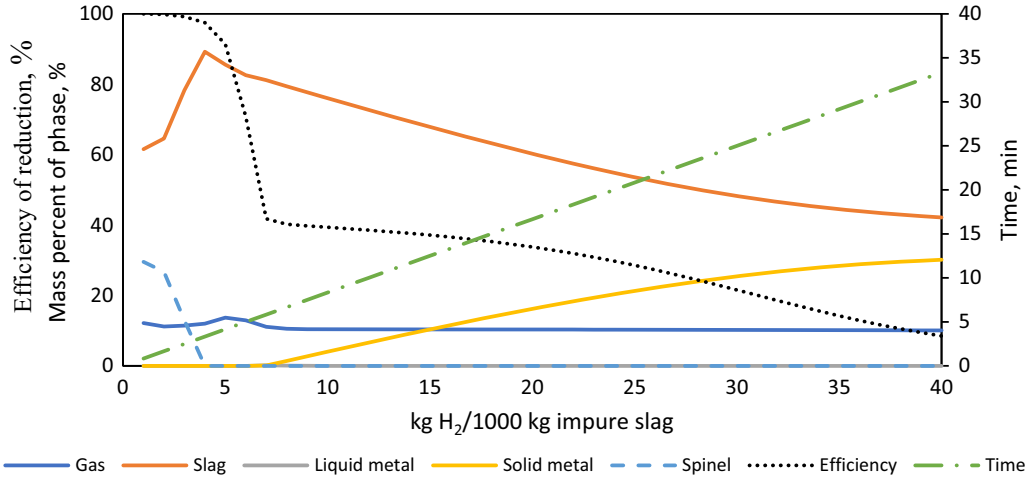

Fig. 14—Mass of phases obtained from impure slag reduction at 1300 °C with 20 vol pct H_2 predicted by FactSage.

produced, are subsequently reacting with the same mixture of H_2 and inert repeatedly for a number of times. Figure 13 shows the flow diagram of how the calculation were performed using FactSage. "Appendix B" shows how the hydrogen input per time input relates to reduction per ton of initial impure slag.

The total mass of the various phases produced are shown in Figure 14. The results show the formation of spinel and slag occur within the first 4 minutes, while the spinel disappears after 4 minutes of reduction. Solid metal, mainly Fe forms after 7 minutes of reduction. It is observed that as time progresses (> 7 minutes), the mass of molten slag decreases and the mass of solid iron increases. Liquid metal was formed between 7 and 9 minutes with a mass less than 0.2 g.

FactSage predicts that at 1300 °C, Pb is fumed from the slag phase to the off-gas flow after 6 minutes. Zn is distributed between spinel and slag within the first 4 minutes and moves to the gas phase from the slag phase. Within the first 3 minutes, As is present in the residue as $AlAsO_4$ moves to the slag phase and is fumed to the gas phase after 6 minutes. Cu present in slag starts

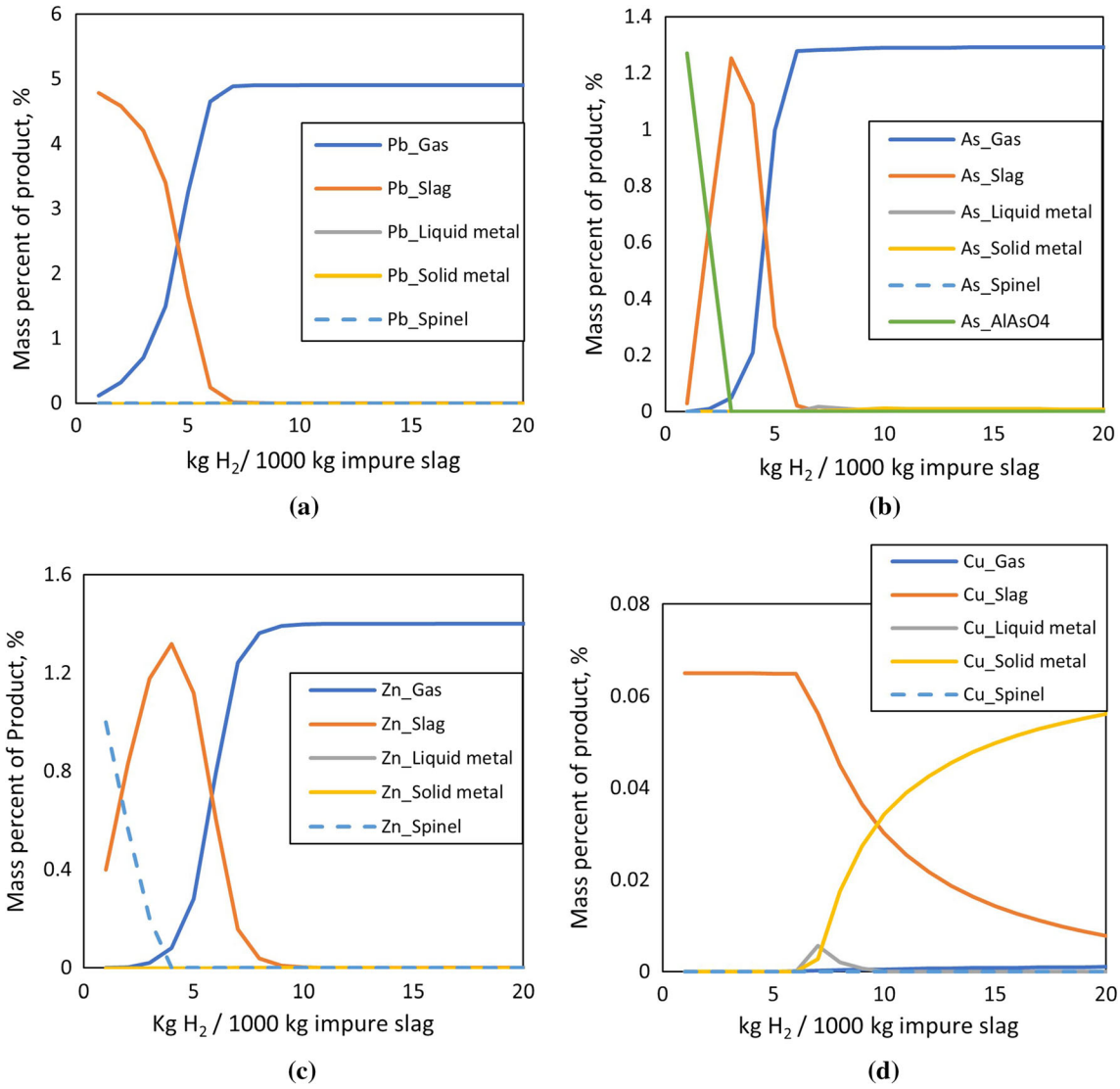

Fig. 15—Elemental distributions of (*a*) Pb, (*b*) As, (*c*) Zn, and (*d*) Cu obtained from impure slag reduction at 1300 °C with 20 vol pct H_2 after 20 minutes predicted by FactSage.

to decrease from 6 minutes and is found in the solid metal after 6 minutes. This theoretical calculation result agrees with the experimental results that were observed at 1300 °C after reduction at 15 minutes and 1 hour of annealing under inert conditions. About 10 pct of the Cu present in the zinc residue is distributed in the liquid metal between 6 and 8 minutes of reduction. Figure 15 shows the elemental distribution of Pb, As, Zn, and Cu as function of added H_2.

The efficiency of the reduction of the hydrogen was calculated using Eq. [1]. The result (shown in Figure 14) reveals that reduction of the impure slag occurs in two steps. In the first stage, there is a sharp decrease in the efficiency in less than 10 minutes. This may be attributed to the conversion of metal oxide present in solid spinel into their metallic state in the liquid metal. As more hydrogen is blown on the sample, FactSage predicts that solid metal which is predominantly iron is formed. The second step is due to the formation of solid iron.

$$\text{Efficiency of reduction} = \frac{n_{H_2O}}{n_{H_2O} + n_{H_2}}, \qquad [1]$$

where n_{H_2O} and n_{H_2} are amounts of water and hydrogen in product, respectively.

For industrial application, the generation of solid iron is an important boundary condition. It is important to as much as possible prevent the formation of solid since other it is very difficult to separate other important elements like copper which dissolves in it. In continuous industrial operation, the formation of solid product is not desired as it may form accretions within the vessel and decreases its volume. Figure 16 shows the distribution of Fe present in the iron residue during reduction. It can be seen the all the iron present in the spinel phase moves to the slag phase. As reduction proceeds, solid iron starts to form from the slag and continues to increase.

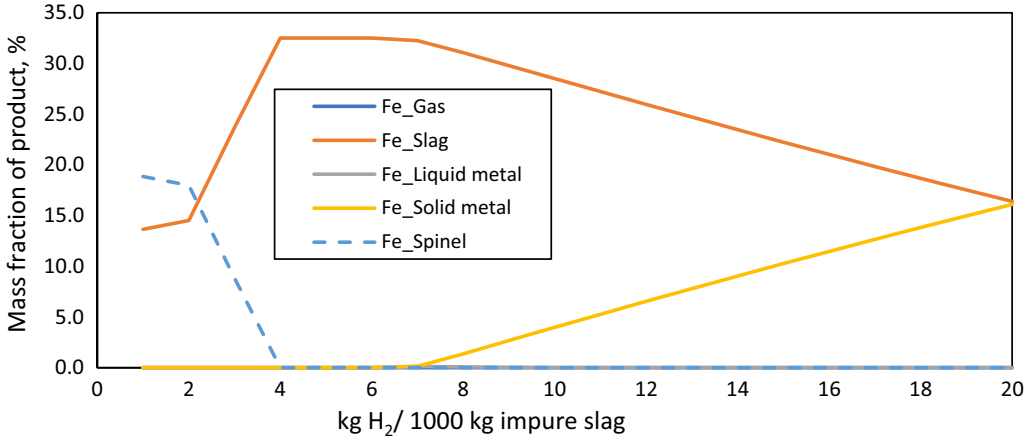

Fig. 16—Elemental distributions of Fe obtained from impure slag reduction at 1300 °C with 20 vol pct H_2 after 20 minutes predicted by FactSage.

E. *Summary*

Iron residue obtained from zinc processing was treated using pyrometallurgical techniques. Oxidation and reduction were carried out on pretreated feed material. This study focused on using hydrogen as reducing agent in experiments and thermodynamic modeling. In the experiment, speiss was formed after 10 minutes. While the percentage of different species of speiss largely vary, it consists mainly of Pb, As, Sb, Ni, and Fe. As time and temperature increased Pb and other volatile metals percentage in the slag were expected to decrease as they move into the gas phase or speiss. However, EPMA analysis showed that Pb and Zn were still present in slag although part of it deports to the speiss. This inconsistency was attributed to error during sampling the feed material or selecting the cross section to be analyzed. Also, the speiss composition varies from one droplet to another, and the speiss size is also quite small (and they are heterogeneous), which all contribute to the error in the analyses. In order to compare experimental results to thermodynamic modeling, another set of tests were performed at 1300 °C, where the samples were left in the furnace for 60 minutes after reduction under N_2 flow. It was assumed that reaction with external sources were absent during this stage although the inert gas contains very small amount of oxygen (< 3 ppm). Moreover, considering the amount of oxygen fed into work tube along with the inert gas, the amount of volatilized PbO may be rather small. This was to ascertain if volatile element would be moved into the gas phase giving sufficient time. Also, this was done in an attempt to achieve equilibrium to compare the results from this set to thermodynamic modeling. In some industrial processes in non-ferrous industries, where the metal formation is very small compared to the amount of slag, the metal is tapped less frequently while the slag is tapped more often.

Thermodynamic modeling was performed in the aim of simulating the reaction for industrial application. In the first instance, the oxygen partial pressure was varied in order to predict the expected products. Therefore, in this case, the formation of a gas phase is minimal and does not fully reflect the volatilization behavior of various elements. The results show the formation of two liquid metals and solid iron at $P(O_2) < 10^{-11}$. In the reduction test where the samples were left in the furnace for 1 hour, the micrographs reveal the formation of speiss consisting of two phases which agrees with FactSage prediction at $P(O_2) < 10^{-10}$.

Another instance was considered where H_2 reacts with the product obtained after oxidation. Gas formed is excluded and the remaining product is reacted with the same amount of H_2. The rationale for this kind of reaction is to simulate the reaction in a furnace where the gas produced exits as off gas and hydrogen reacts with the sample. This idea has been connected to time factor. The volatilization behavior in this case is better shown. The calculations may partly simulate conditions of entrained speiss droplets in the slag, where volatilization is kinetically hindered. Due to the dominant presence of Fe compared to other elements, the reduction of Fe oxides to metallic Fe will proceed with rather small increases of H_2 after the other more noble metals (and ferric oxide) have been reduced.

In the experiments with H_2, $P(O_2)$ is not fixed and will decrease until an apparent equilibrium or steady state where both Fe and FeO are present, thus buffering the $P(O_2)$ until all FeO has been reduced to Fe. In Section III–D–1, Figure 9 shows an expected end state if the $P(O_2)$ is controlled or buffered by, for example, reducing the sample with mixed CO/CO_2 or H_2/H_2O gas. If the $P(O_2)$ of the input gas is fixed to values above the formation of metallic iron, one can control that reduction does not proceed to forming major amounts

of metallic iron. However, if the gas reductant is pure H_2 or H_2 + inert gas, $P(O_2)$ will not be controlled, but will vary and be set by the oxidation state of the metal elements in the slag. In that case, the slag reduction needs to be controlled by the rate limiting factors.

The experiments and thermodynamic model each gives a different perspective and presents a challenge in attempting to ascertain feasibility of using H_2 as reducing agent. While experiments provide good insight of understanding the kinetics of the reaction process, issues arise with sampling good enough representation of the input material which has similar composition for the various test. Moreover, errors also come about when selecting the appropriate cross section for analysis. On the other hand, using FactSage models predicts the products at the end of the reaction without taking into account the reaction kinetics and mass transfer challenges. Both experiments and thermodynamic modeling with FactSage have been used to get a better understanding of reduction of iron residue with hydrogen.

IV. CONCLUSIONS

The use of hydrogen as a reducing agent in the pyrometallurgical treatment of impure non-ferrous slag was investigated in this study. The iron residue was pretreated using air at 700 °C. The metals present in the residue were converted to metal oxides and sulfur content was further decreased to < 1 wt pct during the subsequent oxidation stage within 1200 °C to 1300 °C temperature. After oxidation, the melt was reduced using hydrogen in a 20 vol pct mixture with nitrogen at temperatures 1200 °C, 1250 °C, and 1300 °C. The results revealed that reduction progresses far enough to form speiss droplets already after 10 minutes at all temperatures. Small speiss droplets were formed at different areas within the slag, and after some degree of coalescing, they settled towards the bottom of the crucible.

Thermodynamic modeling was carried out using FactSage at different temperatures and varying oxygen partial pressures. Since FactSage predicts similar products for all the reduction temperatures, 1300 °C was selected as the representative temperature. The results at 1300 °C reveal that at higher $P(O_2)$ ($> 10^{-6.8}$ atm), the residue mainly consists of slag and spinel. Liquid metal forms at oxygen partial pressures lower than $10^{-8.2}$ atm, although very small amounts (1 mg) start to form at $10^{-7.2}$ atm. Further reduction to $P(O_2) < 10^{-11}$ atm results in the formation of solid metal, which is predominantly (> 98 pct) Fe.

ACKNOWLEDGMENTS

This study received financial support from Aalto University, School of Chemical Engineering and Business Finland funded Tocanem Program (41778/31/2020). The utilization of the Academy of Finland's RawMatTERS Finland Infrastructure (RAMI) based at Aalto University, GTK in Espoo is appreciated.

CONFLICT OF INTEREST

On behalf of the of all authors, the corresponding author states that there is no conflict of interest.

FUNDING

Open Access funding provided by Aalto University.

APPENDICES

APPENDIX A: COMPOSITION OF SLAG OBTAINED BY EPMA

After each test, the products obtained were analyzed with EPMA. Tables II, III, IV, V and VI shows the composition of the phases obtained. The solid phase is mainly iron oxide, and it is found scattered in the slag or at the interface of slag and the crucible. The solid marked with * is found at the edge of the slag and crucible and contain higher amount of Mg.

Table AII. Average Phase Composition Obtained from EPMA After Oxidation of Iron Residue for 1 Hour, Wt Pct

Element	1200 °C		1250 °C		1300 °C	
	Slag	Solid	Slag	Solid	Slag	Solid
O	37.23	29.32	38.33	28.24	38.33	29.19
Na	4.24	0.30	2.41	0.51	2.67	0.46
Mg	1.35	1.56	1.74	2.94	3.01	4.69
Al	1.14	0.20	0.93	0.17	0.84	0.23
Si	15.99	0.02	19.11	0.04	18.13	0.03
S	0.13	0.00	0.02	0.00	0.04	0.02
K	0.55	0.00	0.41	0.00	0.43	0.00
Ca	13.07	0.15	9.03	0.10	8.20	0.09
Mn	0.04	0.06	0.04	0.08	0.03	0.07
Fe	16.55	65.97	20.37	64.07	20.50	61.81
Ni	0.01	0.07	0.00	0.11	0.01	0.12
Zn	1.56	1.97	1.23	3.55	1.15	3.14
As	1.29	0.05	1.07	0.05	0.98	0.03
Sb	0.05	0.15	0.08	0.00	0.07	0.00
Ba	1.41	0.01	0.93	0.00	0.87	0.00
Pb	5.26	0.07	4.25	0.04	4.70	0.05

Table AIII. Average Phase Compositions Obtained from EPMA After Reduction at 1200 °C, Wt Pct

Element	5 Minutes		10 Minutes			15 Minutes			20 Minutes		
	Slag	Solid	Slag	Solid	Metal Alloy	Slag	Solid*	Metal Alloy	Slag	Solid*	Metal Alloy
O	35.02	28.15	34.80	25.15	2.67	37.12	28.61	1.03	37.26	28.94	0.96
Na	3.79	0.19	3.98	0.28	0.00	2.75	0.15	0.00	2.82	0.17	0.00
Mg	2.84	2.07	2.80	4.39	0.00	2.76	11.86	0.02	2.65	17.52	0.03
Al	1.02	0.38	1.07	0.18	0.00	0.85	0.11	0.21	0.88	0.19	0.03
Si	14.82	0.06	14.39	0.08	0.75	18.94	0.07	0.00	18.71	0.03	0.00
S	0.04	0.00	0.04	0.01	0.01	0.01	0.00	0.01	0.01	0.00	0.01
K	0.49	0.00	0.50	0.00	0.00	0.44	0.00	0.00	0.44	0.00	0.00
Ca	11.40	0.18	11.64	0.17	0.07	8.03	0.06	0.02	8.39	0.04	0.00
Mn	0.05	0.03	0.04	0.05	0.00	0.04	0.02	0.00	0.04	0.03	0.01
Fe	22.80	67.51	24.87	67.81	0.42	22.91	57.89	2.26	24.49	51.75	1.82
Ni	0.01	0.04	0.01	0.07	0.00	0.01	0.12	6.06	0.00	0.08	3.48
Zn	1.71	1.26	1.72	1.70	0.06	1.33	1.06	0.08	1.14	1.22	0.05
As	0.77	0.04	0.49	0.02	2.66	0.37	0.00	40.09	0.13	0.00	46.93
Sb	0.09	0.00	0.06	0.00	4.25	0.05	0.00	8.29	0.01	0.00	7.88
Ba	1.23	0.02	1.31	0.01	0.00	0.85	0.00	0.02	0.91	0.00	0.00
Pb	3.84	0.05	2.20	0.06	88.38	3.49	0.06	7.02	2.09	0.06	32.22

Table AIV. Average Phase Compositions Obtained from EPMA After Reduction at 1250 °C, Wt Pct

Element	5 Minutes		10 Minutes			15 Minutes			20 Minutes		
	Slag	Solid	Slag	Solid	Metal Alloy	Slag	Solid*	Metal Alloy	Slag	Solid*	Metal Alloy
O	37.53	28.21	34.30	29.22	0.66	36.11	29.01	0.42	38.50	34.29	1.53
Na	2.82	0.38	3.34	0.47	0.00	2.60	0.16	0.00	2.90	0.14	0.00
Mg	3.53	4.26	3.42	6.17	0.00	4.06	20.01	0.01	4.21	22.93	0.01
Al	0.86	0.21	0.94	0.30	0.03	0.84	0.22	0.08	0.89	0.11	0.00
Si	19.73	0.04	13.88	2.68	0.00	18.26	0.02	0.00	19.15	7.88	0.00
S	0.01	0.02	0.02	0.01	0.03	0.00	0.00	0.02	0.00	0.00	0.01
K	0.46	0.00	0.46	0.11	0.00	0.43	0.00	0.00	0.47	0.00	0.00
Ca	8.07	0.08	9.79	2.31	0.01	7.85	0.03	0.00	8.28	0.35	0.00
Mn	0.04	0.06	0.05	0.05	0.00	0.04	0.02	0.01	0.04	0.03	0.00
Fe	19.13	63.88	27.36	56.41	0.40	23.13	49.35	1.81	22.64	33.27	0.18
Ni	0.01	0.09	0.01	0.12	5.53	0.01	0.07	16.39	0.00	0.04	0.67
Zn	1.24	2.67	1.49	1.03	0.01	1.29	1.06	0.01	0.76	0.95	0.01
As	0.78	0.03	0.56	0.08	10.11	0.45	0.00	32.47	0.07	0.00	6.79
Sb	0.07	0.00	0.06	0.02	2.89	0.07	0.00	4.28	0.00	0.00	4.99
Ba	0.87	0.00	1.06	0.26	0.00	0.84	0.00	0.00	0.91	0.00	0.00
Pb	4.79	0.04	3.20	0.66	70.51	3.95	0.04	24.70	1.17	0.03	81.96

Table AV. Average Phase Compositions Obtained from EPMA After Reduction at 1300 °C, Wt Pct

Element	5 Minutes		10 Minutes			15 Minutes			20 Minutes		
	Slag	Solid	Slag	Solid*	Metal Alloy	Slag	Solid*	Metal Alloy	Slag	Solid*	Metal Alloy
O	37.33	28.56	36.95	27.86	1.30	38.03	30.13	0.89	37.06	28.91	1.04
Na	2.66	0.25	2.94	0.18	0.00	2.62	0.11	0.00	2.48	0.16	0.00
Mg	5.01	4.43	4.95	14.10	0.00	5.37	24.80	0.012	5.69	20.87	0.01
Al	0.84	0.26	0.87	0.25	0.00	0.83	0.17	0.007	0.83	0.28	0.00
Si	18.54	0.04	17.40	0.13	0.09	18.54	0.03	0.001	18.35	0.08	0.00
S	0.01	0.00	0.00	0.00	0.00	0.00	0.00	0.011	0.00	0.00	0.02
K	0.43	0.00	0.44	0.00	0.00	0.42	0.00	0.000	0.40	0.00	0.00
Ca	7.85	0.06	8.22	0.06	0.00	7.71	0.02	0.001	7.64	0.02	0.00
Mn	0.04	0.04	0.04	0.03	0.00	0.04	0.03	0.003	0.04	0.03	0.01
Fe	21.23	64.33	23.99	56.06	0.39	22.16	43.91	0.92	23.16	48.41	2.71
Ni	0.01	0.08	0.00	0.08	1.50	0.00	0.06	1.432	0.00	0.06	1.00
Zn	1.24	1.85	1.13	1.23	0.01	1.10	0.69	0.007	1.08	1.17	0.02
As	0.50	0.02	0.14	0.00	9.89	0.15	0.00	28.39	0.23	0.00	29.19
Sb	0.06	0.00	0.02	0.00	6.08	0.00	0.00	6.40	0.01	0.00	5.16
Ba	0.85	0.00	0.91	0.00	0.00	0.82	0.00	0.019	0.80	0.00	0.00
Pb	3.35	0.05	1.97	0.03	75.20	2.19	0.05	49.11	2.22	0.03	55.29

Table AVI. Average Phase Compositions Obtained from EPMA After Reduction at 1300 °C in Addition to 1 Hour Under Inert Condition, Wt Pct

Element	5 Minutes		10 Minutes		15 Minutes				20 Minutes		
	Slag	Solid	Slag	Solid	Slag	Solid*	Pb rich	Fe–As	Slag	Solid*	Fe–As
O	36.70	28.74	36.70	27.43	36.68	26.53	3.35	0.34	36.88	28.28	0.30
Na	3.37	0.12	3.37	0.11	3.28	0.10	0.00	0.00	3.27	0.05	0.00
Mg	6.74	4.20	6.74	9.34	6.67	13.11	0.00	0.01	6.52	18.36	0.01
Al	0.98	0.76	0.98	0.28	0.98	0.09	0.00	0.00	0.99	0.09	0.00
Si	14.23	0.06	14.23	0.13	14.58	0.05	0.01	0.00	14.69	0.01	0.00
S	0.00	0.00	0.00	0.00	0.02	0.00	0.02	0.06	0.03	0.00	0.06
K	0.45	0.00	0.45	0.00	0.46	0.00	0.00	0.00	0.48	0.00	0.00
Ca	10.33	0.09	10.33	0.12	10.10	0.11	0.31	0.01	10.17	0.04	0.03
Mn	0.04	0.04	0.04	0.04	0.05	0.06	0.00	0.00	0.05	0.05	0.01
Fe	25.23	64.96	25.23	61.85	25.61	59.54	0.21	54.28	25.70	53.03	49.11
Ni	0.01	0.05	0.01	0.08	0.00	0.01	0.00	2.66	0.00	0.01	4.63
Zn	0.42	0.91	0.42	0.51	0.19	0.29	0.00	0.00	0.02	0.01	0.00
As	0.08	0.01	0.08	0.00	0.01	0.04	0.05	34.74	0.02	0.03	35.82
Sb	0.03	0.00	0.03	0.00	0.00	0.00	5.70	2.92	0.00	0.00	5.35
Ba	1.12	0.00	1.12	0.00	1.10	0.00	0.00	0.00	1.11	0.00	0.00
Pb	0.19	0.06	0.19	0.05	0.23	0.05	89.74	0.24	0.05	0.05	0.10

APPENDIX B: CALCULATIONS SHOWING HOW MUCH HYDROGEN IS REACTED WITH THE IRON (ZINC CALCINE LEACH) RESIDUE

Total flowrate of gas = 400 mL/min,

Flowrate of hydrogen = 0.2×400 mL/min = 80 mL/min = 0.08 L/min,

Amount of hydrogen = $\frac{0.08}{22.4}$ = 0.0036 mol/min,

where 22.4 L is the molar volume of ideal gas at standard temperature and pressure.

Mass of H_2 = 0.0036 mol/min × 2 g/mol = 0.007 g/min,

where 2 g/mol is the molar mass of hydrogen gas (H_2).

Flowrate of Argon = 0.8×400 = 320 mL/min = 0.32 L/min,

Amount of Argon = $\frac{0.32}{22.4}$ = 0.0143 mol/min,

Mass of Ar = 0.0143 mol/min × 39.95 g/mol = 0.571 g/min,

where 39.95 is the molar mass of argon (Ar).

Mass fraction of hydrogen = $\frac{0.007}{0.007+0.571}$ = 0.012,

Mass fraction of argon = $\frac{0.571}{0.007+0.571}$ = 0.988.

In FactSage calculations, 10 g of a mixture of hydrogen and argon is reacted with 100 g of the iron residue. This implies that 0.012×10 g = 0.12 g of H_2 was used every minute. Hence, for 1000 kg of zinc leach residue, 1.2 kg of hydrogen per minute was used in the calculation.

REFERENCES

1. J. Dang, K.C. Chou, X.J. Hu, and G.H. Zhang: *Steel Res. Int.*, 2013, vol. 84, pp. 526–33.
2. S. Luidold and H. Antrekowitsch: *J. Miner. Met. Mater. Soc.*, 2007, vol. 59, pp. 20–26.
3. C. Yilmaz, J. Wendelstorf, and T. Turek: *J. Clean. Prod.*, 2017, vol. 154, pp. 488–501.
4. K. Rechberger, A. Spanlang, A.S. Conde, H. Wolfmeir, and C. Harris: *Steel Res. Int.*, 2020, vol. 91, pp. 1–10.
5. D. Spreitzer and J. Schenk: *Steel Res. Int.*, 2019, vol. 108, pp. 1–17.
6. A. Pineau, N. Kanari, and I. Gaballah: *Thermochim. Acta*, 2006, vol. 447, pp. 89–100.
7. World Steel Association: World Steel Association, 2021, pp. 1–3. https://www.worldsteel.org/en/dam/jcr:2f02dcdb-9ae8-46e1-ae05-a9797b03d6bd/Hydrogen_vf.pdf. Accessed 10 November 2021.
8. M. Bahgat and M.H. Khedr: *Mater. Sci. Eng. B*, 2007, vol. 138, pp. 251–58.
9. A.A. El-Geassy, F.O. El-Kashif, M.I. Imasr, and A.A. Omar: *ISIJ Int.*, 1994, vol. 34, pp. 541–47.
10. A.A. El-Geassy and V. Rajakumar: *Trans. Iron Steel Inst. Jpn*, 1985, vol. 25, pp. 449–58.
11. J.O. Edström: *J. Iron Steel Inst.*, 1953, vol. 175, pp. 289–304.
12. D. Liu, X. Wang, J. Zhang, Z. Liu, K. Jiao, and X.R. Wang: *Metall. Res. Technol.*, 2017, vol. 114, pp. 1–9.
13. A. Pappu, M. Saxena, and S.R. Asolekar: *Sci. Total Environ.*, 2006, vol. 359, pp. 232–43.
14. A.D. De Souza, P.S. Pina, and V.A. Leao: *Miner. Eng.*, 2007, vol. 20, pp. 591–99.
15. M.R.C. Ismael and J.M.R. Carvalho: *Miner. Eng.*, 2003, vol. 16, pp. 31–39.
16. M. Kerolli-Mustafa, L. Ćurković, H. Fajković, and S. Rončević: *Croat. Chem. Acta*, 2015, vol. 88, pp. 189–96.
17. Y. Wang, H. Yang, G. Zhang, J. Kang, and C. Wang: *Chem. Eng. J. Adv.*, 2020, vol. 23, pp. 1–8.
18. S. Ju, Y. Zhang, Y. Zhang, P. Xue, and Y. Wang: *J. Hazard. Mater.*, 2011, vol. 192, pp. 554–58.
19. J. Wood, J. Coveney, G. Helin, L. Xu, and S. Xincheng: *Proc. EMC*, 2015.
20. J. Hoang, M.A. Reuter, R. Matusewicz, S. Hughes, and N. Piret: *Miner. Eng.*, 2009, vol. 22, pp. 742–51.
21. H. Han, W. Sun, Y. Hu, B. Jia, and H. Tang: *J. Hazard. Mater.*, 2014, vol. 278, pp. 49–54.
22. E. Abkhoshk, E. Jorjani, M.S. Al-Harahsheh, F. Rashchi, and M. Naazeri: *Hydrometallurgy*, 2014, vol. 149, pp. 153–67.
23. P. Asokan, M. Saxena, and S.R. Asolekar: *Mater. Charact.*, 2010, vol. 61, pp. 1342–55.
24. E.H.M. Moors and G.P.J. Dijkema: *Technol. Forecast. Soc. Change*, 2006, vol. 73, pp. 250–65.
25. A. Ruşen, A.S. Sunkar, and Y.A. Topkaya: *Hydrometallurgy*, 2008, vol. 93, pp. 45–50.
26. C. Arslan and F. Arslan: *Turk. J. Eng. Environ. Sci.*, 2003, vol. 27, pp. 45–52.
27. M. Rinne: Masters' Thesis, Aalto University, 2019.
28. S. Creedy, A. Glinin, R. Matusewicz, S. Hughes, and M. Reuter: *World Metall. ERZMETALL*, 2013, vol. 4, pp. 230–35.
29. M. Rämä, S. Nurmi, A. Jokilaakso, L. Klemettinen, P. Taskinen, and J. Salminen: *Metals (Basel)*, 2018, vol. 9, p. 744.
30. A. Toropainen: Masters' Thesis, Aalto University, 2016.
31. S. Nurmi: Masters' Thesis, Aalto University, 2018.
32. N. Hellstén, L. Klemettinen, D. Sukhomlinov, H.O. Brien, P. Taskinen, A. Jokilaakso, and J. Salminen: *J. Sustain. Metall.*, 2019, vol. 5, pp. 463–73.
33. R.L. Frost, M.L. Weier, and W. Martens: *J. Therm. Anal. Calorim.*, 2005, vol. 82, pp. 115–18.
34. S. Steinlechner and J. Antrekowitsch: *Metals (Basel)*, 2018, vol. 8, p. 335.
35. M. Rämä: Masters' Thesis, Aalto University, 2017.
36. J. Chaidez-Felix, A. Romero-Serrano, A. Hernandez-Ramirez, M. Perez-Labra, I. Almaguer-Guzman, R. Benavides-Perez, and M. Flores-Favela: *Trans. Nonferr. Met. Soc. China*, 2014, vol. 4, pp. 120–29.
37. J. Isaksson, T. Vikström, A. Lennartsson, and C. Samuelsson: *Metals (Basel)*, 2021, vol. 11, p. 992.
38. J. Isaksson, T. Vikström, A. Lennartsson, A. Andersson, and C. Samuelsson: *Metals (Basel)*, 2021, vol. 11, p. 1098.
39. C.W. Bale, E. Bélisle, P. Chartrand, S.A. Decterov, G. Eriksson, A.E. Gheribi, K. Hack, I. Jung, Y. Kang, J. Melançon, A.D. Pelton, S. Petersen, C. Robelin, J. Sangster, P. Spencer, and M. Van Ende: *CALPHAD*, 2016, vol. 54, pp. 35–53.